$1/f$ noise of a nanopillar tunnel-magnetoresistance sensor originating from a wide distribution of bath correlation times

Hiroshi Imamura,[*] Hiroko Arai,[†] Rie Matsumoto, and Toshiki Yamaji
Research Center for Emerging Computing Technologies (RCECT), National Institute of Advanced Industrial Science and Technology (AIST), Tsukuba, Ibaraki 305-8568, Japan

(Received 6 December 2023; revised 16 April 2024; accepted 25 June 2024; published 12 July 2024)

The tunnel magnetoresistance (TMR) sensor is a highly sensitive magnetic field sensor that is expected to be applied in various fields, such as magnetic recording, industrial sensing, and biomedical sensing. To improve the detection capability of TMR sensors in the low-frequency regime, it is necessary to suppress the $1/f$ noise. We theoretically study the $1/f$ noise of a tiny TMR sensor using the macrospin model. Starting from the generalized Langevin equation, the $1/f$ noise power spectrum and the Hooge parameter are derived. The calculated Hooge parameter of a tiny TMR sensor is much smaller than that of a conventional TMR sensor with large junction area. The results provide a new perspective on magnetic $1/f$ noise and will be useful for improving TMR sensors.

DOI: 10.1103/PhysRevApplied.22.014032

I. INTRODUCTION

The tunnel-magnetoresistance (TMR) sensor [1–7] is a highly sensitive magnetic field sensor where the magnetic field signal is converted to a change in resistance of a magnetic tunnel junction (MTJ) [8–12]. The most popular application of the TMR sensor is the reading head of hard-disk drives. Because of their high sensitivity, small size, and low power consumption, TMR sensors are expanding their applications into a variety of fields, such as industrial sensing and biomedical sensing. In biomedical applications such as magnetocardiography and magnetoencephalography, TMR sensors detect the weak magnetic fields generated in the human heart and brain by electrophysiological activity of cardiac muscle and nerve cells [4–6]. The frequency range of the biomagnetic signal is less than a few hundred hertz, where the $1/f$ noise is the dominant noise. Reduction of $1/f$ noise is a key issue for biomedical applications [3,13].

$1/f$ noise is a ubiquitous low-frequency noise, the noise power of which is inversely proportional to the frequency, f [14–17]. A large number of theories have been developed to explain the mechanism of $1/f$ noise, as reviewed in Ref. [17]. An obvious way to obtain a $1/f$ power spectrum is to superimpose a large number of Lorentzian power spectra produced by exponential relaxation processes [14,17–20]. The magnitude of the $1/f$ noise in different devices and materials is characterized by the Hooge parameter [15].

The magnetic $1/f$ noise derived from the thermal fluctuation of magnetization in a TMR sensor has been studied by several groups [2,7,21–28]. In most previous studies, the TMR sensors exhibit clear hysteresis in the magnetic field dependence of resistance, and the $1/f$ noise is observed within the hysteresis loop. The observed $1/f$ noise has been attributed to thermally excited hopping of magnetic domain walls between pinning sites. It is natural to ask the question whether magnetic $1/f$ noise appears in a tiny TMR sensor, where domain walls cannot be created. If $1/f$ noise appears in tiny TMR sensors, what is its power? To answer this question, it is necessary to develop a theoretical model of magnetic $1/f$ noise based on the macrospin model.

In this paper, we propose a theoretical model for the magnetic $1/f$ noise of a tiny TMR sensor based on the macrospin model. Starting from the generalized Langevin equation, we derive an analytical expression for the voltage power spectrum in the low-frequency regime. Assuming a wide distribution of bath correlation times, the derived voltage power spectrum is inversely proportional to the frequency, i.e., $1/f$ noise. We also show that the Hooge parameter of a tiny TMR sensor is much smaller than that of a conventional TMR sensor with large junction area.

II. THEORETICAL MODEL

The system we consider is the MTJ nanopillar shown in Fig. 1(a), which is the core element of a tiny TMR sensor. The nonmagnetic insulating layer is sandwiched between ferromagnetic layers. The top ferromagnetic layer is the free layer (FL), the magnetization of which is softly pinned by the orange-peel coupling field, $\boldsymbol{H}_p$, directed in the z

[*]Contact author: h-imamura@aist.go.jp
[†]Contact author: arai-h@aist.go.jp

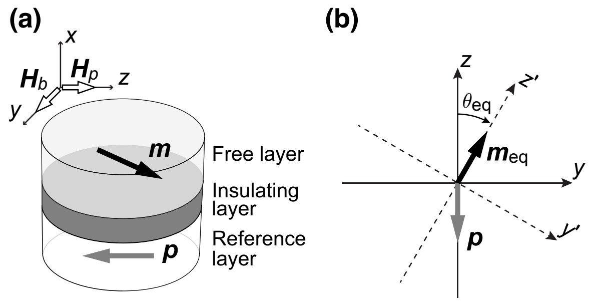

FIG. 1. (a) Schematic illustration of a magnetic tunnel junction. The insulating layer is sandwiched by the free layer (FL) and the reference layer (RL). The direction of the magnetization in the FL is denoted by the magnetization unit vector, $\boldsymbol{m}$. The direction of the magnetization in the RL is denoted by the magnetization unit vector, $\boldsymbol{p}$, and is fixed in the negative z direction. The magnetization in the FL is pinned by the orange-peel coupling field, $\boldsymbol{H}_p$, directed in the z direction, and by the uniaxial anisotropy field along the z axis. The bias field, $\boldsymbol{H}_b$, is applied in the y direction. (b) Definition of the rotated coordinate system. The z' axis is aligned to the equilibrium direction of the magnetization in the FL, $\boldsymbol{m}_{\text{eq}}$, by rotating around the x axis by angle θ_{eq}.

direction, and by the uniaxial anisotropy field, H_k, along the z axis. The direction of the magnetization in the FL is denoted by $\boldsymbol{m}$. To tune the sensitivity, the bias field, $\boldsymbol{H}_b$, is applied in the y direction. The bottom ferromagnetic layer is the reference layer (RL), the magnetization unit vector, $\boldsymbol{p}$, of which is fixed in the negative z direction [7]. The size of the TMR sensor is assumed to be so small that a domain wall cannot be created in the FL, i.e., about or less than 10 nm.

Assuming that the FL is a thin circular disk, the magnetic free-energy density of the FL is given by

$$E = -\mu_0 M_s \boldsymbol{m} \cdot (\boldsymbol{H}_p + \boldsymbol{H}_b) + \frac{1}{2}\mu_0 M_s^2 m_x^2 - \frac{1}{2}\mu_0 M_s H_k m_z^2, \tag{1}$$

where μ_0 is the permeability of vacuum, and M_s is the saturation magnetization. The equilibrium direction, $\boldsymbol{m}_{\text{eq}} = (0, \sin\theta_{\text{eq}}, \cos\theta_{\text{eq}})$, is obtained by minimizing E.

The voltage noise of the TMR sensor is induced by the resistance variation due to fluctuation of $\boldsymbol{m}$ around the equilibrium direction. To calculate the fluctuation of $\boldsymbol{m}$, we introduce the rotated coordinate system shown in Fig. 1(b), where the y' and z' axes are generated by rotating the y and z axes around the x axis by the angle θ_{eq}. The basis vectors of the x–y'–z' coordinate system are defined as

$$\begin{pmatrix} \boldsymbol{e}_x \\ \boldsymbol{e}_{y'} \\ \boldsymbol{e}_{z'} \end{pmatrix} = \begin{pmatrix} 1 & 0 & 0 \\ 0 & \cos\theta_{\text{eq}} & -\sin\theta_{\text{eq}} \\ 0 & \sin\theta_{\text{eq}} & \cos\theta_{\text{eq}} \end{pmatrix} \begin{pmatrix} \boldsymbol{e}_x \\ \boldsymbol{e}_y \\ \boldsymbol{e}_z \end{pmatrix}. \tag{2}$$

In the rotated coordinate system, the magnetization unit vector in the FL is represented as

$$\boldsymbol{m} = m_x \boldsymbol{e}_x + m_{y'} \boldsymbol{e}_{y'} + m_{z'} \boldsymbol{e}_{z'}. \tag{3}$$

Since we are interested in the small fluctuation of $\boldsymbol{m}$ around $\boldsymbol{m}_{\text{eq}}$, we assume $|m_x| \ll 1$, $|m_{y'}| \ll 1$, and $|m_{z'}| \simeq 1$.

The resistance of the TMR sensor is given by [8,9,29]

$$R = R_0 + \frac{\bar{R}}{1 + P^2 \boldsymbol{m} \cdot \boldsymbol{p}}, \tag{4}$$

where R_0 is the resistance not caused by tunneling, $\bar{R}$ is the resistance due to tunneling at $\boldsymbol{m} \cdot \boldsymbol{p} = 0$, and P is the spin polarization of tunneling electrons. Substituting Eq. (3) into Eq. (4), the resistance is obtained as

$$R = R_0 + \frac{\bar{R}}{1 - P^2(\cos\theta_{\text{eq}}\, m_{z'} - \sin\theta_{\text{eq}}\, m_{y'})}. \tag{5}$$

Up to the first order of $m_{y'}$, the resistance can be approximated as

$$R = R_0 + \frac{\bar{R}}{1 - P^2 \cos\theta_{\text{eq}}} - \frac{\bar{R} P^2 \sin\theta_{\text{eq}}}{(1 - P^2 \cos\theta_{\text{eq}})^2}\, m_{y'}. \tag{6}$$

III. RESULTS

In this section, we show the results of our theoretical analysis of the magnetic $1/f$ noise of a tiny TMR sensor. We first show the relation between the voltage power spectrum and the power spectrum of $m_{y'}$ in Sec. III A. To calculate the power spectrum of $m_{y'}$, we solve the linearized equations of motion of $\boldsymbol{m}$ by using the Fourier transformation in Sec. III B. Then we derive the Lorentzian power spectrum of $m_{y'}$ in Sec. III C. Assuming that the bath correlation time, τ_c, has a wide distribution, we derive the $1/f$ power spectrum of voltage by superimposing the Lorentzian power spectra with different τ_c in Sec. III D. In Sec. III E, we show that the Hooge parameter of a tiny TMR sensor is much smaller than that of a conventional TMR sensor with the same sensitivity by comparison with the experimental results of Ref. [7].

A. Power spectrum of voltage

In most experiments, the voltage noise of a TMR sensor is measured under a constant direct current, I. Assuming that the measured voltage, V, is proportional to the resistance, R, the power spectrum of voltage, $S_{VV}(f)$, is proportional to the power spectrum of resistance, $S_{RR}(f)$, as

$$S_{VV}(f) = I^2 S_{RR}(f). \quad (7)$$

Introducing the angular frequency, $\omega = 2\pi f$, the power spectrum of resistance is defined as

$$S_{RR}(\omega) = 4\int_0^\infty \langle R(t)R(0)\rangle \cos(\omega t)\, dt, \quad (8)$$

where $\langle\cdot\rangle$ represents the statistical average. Substituting Eq. (6) into Eq. (8), $S_{RR}(\omega)$ is expressed as

$$S_{RR}(\omega) = \left[\frac{\bar{R}P^2 \sin\theta_{\mathrm{eq}}}{(1-P^2\cos\theta_{\mathrm{eq}})^2}\right]^2 S_{m_{y'}m_{y'}}(\omega), \quad (9)$$

where $S_{m_{y'}m_{y'}}(\omega)$ is the power spectrum of $m_{y'}$ defined as

$$S_{m_{y'}m_{y'}}(\omega) = 4\int_0^\infty \langle m_{y'}(t)m_{y'}(0)\rangle \cos(\omega t)\, dt. \quad (10)$$

We define the Fourier transform of a function $f(t)$ as $f(\omega) = \int_{-\infty}^{\infty} f(t)\exp(-i\omega t)\, dt$. Substituting the inverse Fourier transform of $m_{y'}$ into Eq. (10) and performing some algebra, we obtain

$$S_{m_{y'}m_{y'}}(\omega) = \frac{1}{2\pi}\int_{-\infty}^{\infty} \langle m_{y'}(\omega)m_{y'}(\omega')\rangle\, d\omega' + \frac{1}{2\pi}\int_{-\infty}^{\infty} \langle m_{y'}(-\omega)m_{y'}(\omega')\rangle\, d\omega'. \quad (11)$$

The Fourier transform of $m_{y'}$ can be obtained by solving the equations of motion in Fourier space.

B. Equations of motion and the Fourier transforms of $\boldsymbol{m_x}$ and $\boldsymbol{m_{y'}}$

The equations of motion of $\boldsymbol{m}$ are given by the generalized Langevin equation [30–32],

$$\dot{\boldsymbol{m}}(t) = -\gamma \boldsymbol{m}(t)\times(\boldsymbol{H}_{\mathrm{eff}} + \boldsymbol{r}) + \alpha \boldsymbol{m}\times\int_{-\infty}^{t} \nu(t-t')\dot{\boldsymbol{m}}(t')\, dt', \quad (12)$$

where $\dot{\boldsymbol{m}}(t)$ is the time derivative of $\boldsymbol{m}(t)$, γ is the gyromagnetic ratio, and α is the Gilbert damping constant. The effective magnetic field acting on $\boldsymbol{m}$ is given by

$$\boldsymbol{H}_{\mathrm{eff}} = -M_s m_x \boldsymbol{e}_x + H_b \boldsymbol{e}_y + (H_p + H_k m_z)\boldsymbol{e}_z. \quad (13)$$

The memory function is defined as

$$\nu(t-t') = \frac{1}{\tau_c}\exp\left(-\frac{|t-t'|}{\tau_c}\right), \quad (14)$$

where τ_c is the bath correlation time. The thermal agitation field, $\boldsymbol{r}$, is a random field satisfying $\langle r_j\rangle = 0$ and

$$\langle r_j r_k\rangle = \frac{\mu}{2}\delta_{j,k}\nu(t-t'), \quad (15)$$

where subscripts j and k denotes x, y, z, y', or z'. The constant μ is defined as

$$\mu = \frac{2\alpha k_B T}{\gamma\mu_0 M_s \Omega}, \quad (16)$$

where k_B is the Boltzmann constant, T is temperature, and Ω is the volume of the FL.

From Eqs. (15) and (16) we see that the magnitude of the thermal agitation field is on the order of $\sqrt{\alpha}$ because μ is on the order of α. The stochastic Landau-Lifshitz-Gilbert (LLG) equation with the Markovian damping derived by Brown [33] is reproduced in the limit of $\tau_c \to 0$ because $\lim_{\tau_c\to 0}\nu(t-t') = 2\delta(t-t')$, where $\delta(t-t')$ is the Dirac delta function. It should be noted that $1/f$ noise cannot be derived from the LLG equation with Markovian damping because many physical processes with different time scales are required to generate $1/f$ noise.

Since the FL of a typical TMR sensor is made of a ferromagnetic material with $\alpha \ll 1$, we focus on terms up to the first order of α in the equations of motion. We also assume that m_x, $m_{y'}$, r_x, $r_{y'}$, and $r_{z'}$ are small enough to linearize the equations of motion in terms of these small variables. Equation (12) can thus be approximated as

$$\dot{m}_x(t) = -\omega_0 m_{y'}(t) + \gamma r_{y'}(t) - \alpha\int_{-\infty}^{t} \nu(t-t')\dot{m}_{y'}(t')\, dt', \quad (17)$$

$$\dot{m}_{y'}(t) = \omega_1 m_x(t) - \gamma r_x(t) + \alpha\int_{-\infty}^{t} \nu(t-t')\dot{m}_x(t')\, dt', \quad (18)$$

$$\dot{m}_{z'}(t) = 0, \quad (19)$$

where

$$\omega_0 = \gamma(H_b\sin\theta_{\mathrm{eq}} + H_p\cos\theta_{\mathrm{eq}} + H_k\cos 2\theta_{\mathrm{eq}}), \quad (20)$$

$$\omega_1 = \gamma(M_s + H_b\sin\theta_{\mathrm{eq}} + H_p\cos\theta_{\mathrm{eq}} + H_k\cos^2\theta_{\mathrm{eq}}). \quad (21)$$

Following Ref. [32], we approximate the non-Markovian damping term in Eqs. (17) and (18) up to the first order of α. Successive application of integration by parts gives the following linearized equations of motion up to the order of α:

$$\dot{m}_x(t) = -\hat{\gamma}_1\omega_0 m_{y'}(t) + \gamma r_{y'}(t) - \tilde{\alpha}\omega_1 m_x(t), \quad (22)$$

$$\dot{m}_{y'}(t) = \hat{\gamma}_0\omega_1 m_x(t) - \gamma r_x(t) - \tilde{\alpha}\omega_0 m_{y'}(t), \quad (23)$$

where

$$\hat{\gamma}_0 = \left(1 + \frac{\alpha\xi_0}{1+\xi_0\xi_1}\right), \quad (24)$$

$$\hat{\gamma}_1 = \left(1 + \frac{\alpha\xi_1}{1+\xi_0\xi_1}\right), \quad (25)$$

$$\tilde{\alpha} = \frac{\alpha}{1+\xi_0\xi_1}, \quad (26)$$

$$\xi_0 = \tau_c\omega_0, \quad \xi_1 = \tau_c\omega_1. \quad (27)$$

Details of the derivation of the above equations will be provided in the Appendix.

In Fourier space, the equations of motion are expressed as

$$i\omega m_x(\omega) = -\hat{\gamma}_1\omega_0 m_{y'}(\omega) + \gamma r_{y'}(\omega) - \tilde{\alpha}\omega_1 m_x(\omega), \quad (28)$$

$$i\omega m_{y'}(\omega) = \hat{\gamma}_0\omega_1 m_x(\omega) - \gamma r_x(\omega) - \tilde{\alpha}\omega_0 m_{y'}(\omega). \quad (29)$$

The solutions are obtained as

$$m_x(\omega) = \frac{\hat{\gamma}_1\omega_0\gamma r_x(\omega) + (\tilde{\alpha}\omega_0 + i\omega)\gamma r_{y'}(\omega)}{A(\omega)}, \quad (30)$$

$$m_{y'}(\omega) = \frac{\hat{\gamma}_0\omega_1\gamma r_{y'}(\omega) - (\tilde{\alpha}\omega_1 + i\omega)\gamma r_x(\omega)}{A(\omega)}, \quad (31)$$

where

$$A(\omega) = (\hat{\gamma}_0\hat{\gamma}_1 + \tilde{\alpha}^2)\omega_0\omega_1 - \omega^2 + i\tilde{\alpha}(\omega_0 + \omega_1)\omega. \quad (32)$$

C. Power spectrum of $m_{y'}$

From Eq. (31), the correlation of $m_{y'}(\omega)$ and $m_{y'}(\omega')$ is expressed as

$$\langle m_{y'}(\omega)m_{y'}(\omega')\rangle = \frac{(\hat{\gamma}_0\omega_1)^2}{A(\omega)A(\omega')}\gamma^2\langle r_{y'}(\omega)r_{y'}(\omega')\rangle + \frac{(\tilde{\alpha}\omega_1 + i\omega)(\tilde{\alpha}\omega_1 + i\omega')}{A(\omega)A(\omega')}\gamma^2\langle r_x(\omega)r_x(\omega')\rangle, \quad (33)$$

where we use the fact that r_x and $r_{y'}$ do not correlate with each other. The correlation $\langle m_{y'}(-\omega)m_{y'}(\omega')\rangle$ is obtained by replacing ω with $-\omega$ in Eq. (33)

Following Ref. [34], the correlation of thermal agitation fields in Fourier space is obtained as

$$\langle r_j(\omega)r_k(\omega')\rangle = 2\pi\mu\delta_{j,k}\frac{1}{1+i\tau_c\omega}\delta(\omega+\omega'). \quad (34)$$

The correlation $\langle r_j(-\omega)r_k(\omega')\rangle$ is obtained by replacing ω with $-\omega$ in Eq. (34).

Substituting Eqs. (33) and (34) into Eq. (11), the power spectrum of $m_{y'}$ is expressed as

$$S_{m_{y'}m_{y'}}(\omega) = \frac{(\hat{\gamma}_0^2 + \tilde{\alpha}^2)\omega_1^2 + \omega^2}{B(\omega)}\frac{2\gamma^2\mu}{1+(\tau_c\omega)^2}, \quad (35)$$

where

$$B(\omega) = [(\hat{\gamma}_0\hat{\gamma}_1 + \tilde{\alpha}^2)\omega_0\omega_1 - \omega^2]^2 + [\tilde{\alpha}(\omega_0+\omega_1)\omega]^2. \quad (36)$$

In the low-frequency regime satisfying $\omega \ll \omega_0$ and $\omega \ll \omega_1$, Eq. (35) can be approximated by the Lorentzian function as

$$S_{m_{y'}m_{y'}}(\omega) = \frac{2\gamma^2\mu}{(\hat{\gamma}_1\omega_0)^2}\frac{1}{1+(\tau_c\omega)^2}. \quad (37)$$

Since ω_0 and ω_1 are on the order of 0.1–10 GHz for conventional TMR sensors [7], the low-frequency condition is clearly satisfied for the frequency range of the biomagnetic signal, i.e., less than a few hundred hertz.

D. Superimposition of Lorentzian power spectra

The bath correlation time, τ_c, is the decay time of the correlation of the thermal agitation field as shown in Eq. (15). The thermal agitation field may be produced by many kinds of sources or baths, such as dipolar coupling with magnons in the reference layer and spin-orbit coupling with phonons. Since τ_c depends on the relaxation mechanism of the bath, different relaxation modes in different baths have their own τ_c. Instead of discussing τ_c for some specific types of baths, we just assume a distribution of τ_c and analyze the effect of the distribution of τ_c on the low-frequency power spectrum of voltage. Assuming a wide distribution of τ_c, we derive an analytical expression of the power spectrum of the magnetic $1/f$ noise.

We assume that τ_c is uniformly distributed in the range of $\tau_{c,\min} \le \tau_c \le \tau_{c,\max}$ and has a probability distribution defined as $\rho(\tau_c) = 1/(\tau_{c,\max} - \tau_{c,\min})$. The superimposition of $S_{m_{y'}m_{y'}}(\omega)$ for all τ_c is given by

$$S_{m_{y'}m_{y'}}(\omega) = \frac{2\gamma^2\mu}{\omega_0^2}\int_0^\infty \frac{1}{\hat{\gamma}_1^2}\frac{\rho(\tau_c)}{1+(\tau_c\omega)^2}d\tau_c. \quad (38)$$

As a function of τ_c, $\hat{\gamma}_1$ is almost unity except around the peak at $\tau_c = 1/\sqrt{\omega_0\omega_1}$, which is on the order of

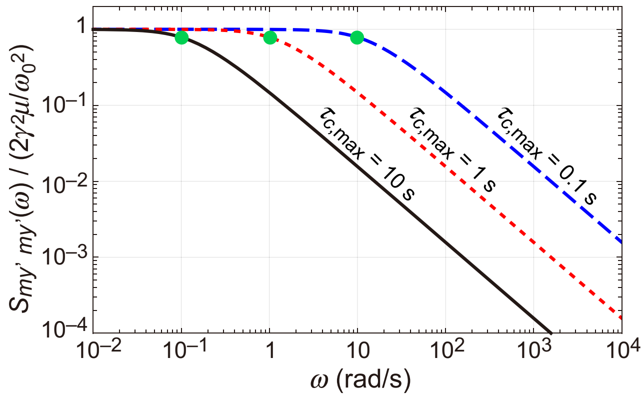

FIG. 2. Power spectrum of $m_{y'}$, $S_{m_{y'}m_{y'}}(\omega)$, given by Eq. (40), normalized by $2\gamma^2\mu/\omega_0^2$. The black solid, red dotted, and blue dashed curves represent the results for $\tau_{c,\max} = 10$, 1, and 0.1 s, respectively. The green circles indicate the values at $\omega = 1/\tau_{c,\max}$.

nanoseconds. Since the peak value of $\hat{\gamma}_1$ is as small as $1 + (\alpha/2)\sqrt{\omega_1/\omega_0}$, and ω is assumed to be much smaller than ω_0 and ω_1, Eq. (38) can be approximated as

$$\begin{aligned} S_{m_{y'}m_{y'}}(\omega) &= \frac{2\gamma^2\mu}{\omega_0^2}\frac{1}{\tau_{c,\mathrm{diff}}}\int_{\tau_{c,\min}}^{\tau_{c,\max}}\frac{1}{1+(\tau_c\omega)^2}\,d\tau_c \\ &= \frac{2\gamma^2\mu}{\omega_0^2}\frac{1}{\tau_{c,\mathrm{diff}}}\left[\frac{\arctan(\omega\tau_{c,\max})}{\omega} - \frac{\arctan(\omega\tau_{c,\min})}{\omega}\right], \end{aligned} \tag{39}$$

where $\tau_{c,\mathrm{diff}} = \tau_{c,\max} - \tau_{c,\min}$. Since $\arctan(x)/x$ is a monotonically decreasing function of x for $x > 0$ and $\lim_{x\to 0}\arctan(x)/x = 1$, $S_{m_{y'}m_{y'}}(\omega)$ is a monotonically decreasing function of ω and takes a maximum value of $2\gamma^2\mu/\omega_0^2$ in the limit of $\omega \to 0$.

When $\omega\tau_{c,\min} \ll 1$, the second term in the square bracket of Eq. (39) can be neglected and $S_{m_{y'}m_{y'}}(\omega)$ is approximated as

$$S_{m_{y'}m_{y'}}(\omega) = \frac{2\gamma^2\mu}{\omega_0^2}\frac{\arctan(\omega\tau_{c,\max})}{\omega\tau_{c,\max}}. \tag{40}$$

Figure 2 shows $S_{m_{y'}m_{y'}}(\omega)$ given by Eq. (40) normalized by $2\gamma^2\mu/\omega_0^2$ for $\tau_{c,\max} = 10$ s (black solid), 1 s (red dotted), and 0.1 s (blue dashed). The values at $\omega = 1/\tau_{c,\max}$ are indicated by the green circles. All curves are almost flat for $\omega \ll 1/\tau_{c,\max}$ and inversely proportional to ω for $\omega \gg 1/\tau_{c,\max}$.

Assuming a wide distribution of τ_c satisfying $\omega\tau_{c,\min} \ll 1$ and $\omega\tau_{c,\max} \gg 1$, we have $\arctan(\omega\tau_{c,\min}) = 0$ and $\arctan(\omega\tau_{c,\max}) = \pi/2$. Then the power spectrum can be approximated as

$$S_{m_{y'}m_{y'}}(\omega) = \frac{2\gamma^2\mu}{\omega_0^2}\frac{1}{\tau_{c,\max}}\frac{\pi}{2\omega}, \tag{41}$$

which is inversely proportional to the angular frequency, ω $(= 2\pi f)$. From Eqs. (7), (9), and (41), the voltage power spectrum is given by

$$S_{VV}(f) = \left[\frac{I\bar{R}P^2\sin\theta_{\mathrm{eq}}}{(1-P^2\cos\theta_{\mathrm{eq}})^2}\right]^2 \frac{\gamma^2\mu}{2\omega_0^2}\frac{1}{\tau_{c,\max}}\frac{1}{f}. \tag{42}$$

This is the *main result* of this paper. The obvious difference from other models of low-frequency magnetic noise [21,23,35–38] is that Eq. (42) has the term $1/\tau_{c,\max}$ as information about the distribution of the bath correlation time. It should be noted that the $1/f$ noise of a tiny TMR sensor that we have derived is the response to thermal agitation fields that exhibit a $1/f$ power spectrum as the superimposition of Lorentzian power spectra.

E. Comparison with a conventional TMR sensor with large junction area

We compare the derived $1/f$ noise of the macrospin model with the experimental results for a conventional TMR sensor with large junction area reported in Ref. [7]. The Hooge parameter, α_H, is a convenient measure to compare the $1/f$ noise between different MTJs, which is defined as

$$S_{VV}(f) = S_{VV}^{\mathrm{wh}} + \alpha_H V_b^2 A^{-1} f^{-1}, \tag{43}$$

where S_{VV}^{wh} is the power spectral density of the white noise, V_b is the bias voltage, and A is the area of the MTJ. The typical value of the Hooge parameter of conventional TMR sensors is about 10^{-6}–10^{-11} $\mu\mathrm{m}^2$ [7,26–28]. From Eq. (6), the bias voltage is given by

$$V_b = I\left(R_0 + \frac{\bar{R}}{1-P^2\cos\theta_{\mathrm{eq}}}\right). \tag{44}$$

From Eqs. (16), (42), (43), and (44), the Hooge parameter of a tiny TMR sensor is obtained as

$$\alpha_H = \left\{\frac{\bar{R}P^2\sin\theta_{\mathrm{eq}}}{(1-P^2\cos\theta_{\mathrm{eq}})[\bar{R}+R_0(1-P^2\cos\theta_{\mathrm{eq}})]}\right\}^2 \times \frac{\alpha\gamma k_B T}{\mu_0 M_s d}\frac{1}{\omega_0^2}\frac{1}{\tau_{c,\max}}, \tag{45}$$

where d is the thickness of the FL.

To compare Eq. (45) with the experimental results of a conventional TMR sensor, we determine the junction parameters by fitting the bias field dependence of the

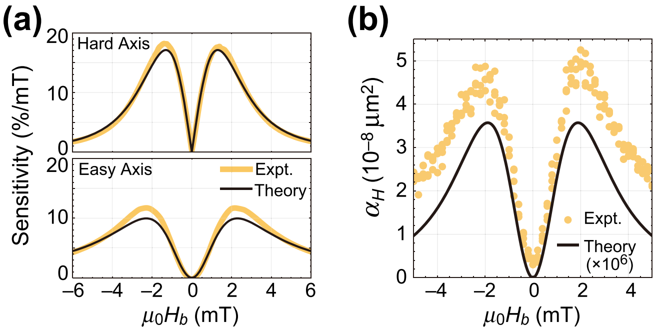

FIG. 3. (a) Sensitivity as a function of the bias field, $\mu_0 H_b$. The upper panel shows the results for the signal field along the magnetization hard axis, i.e., the y axis. The lower panel shows the results for the signal field along the magnetization easy axis, i.e., the z axis. In both panels, the yellow and the black curves represent the experimental and theoretical results, respectively. (b) The Hooge parameter, α_H, as a function of the bias field, $\mu_0 H_b$. The yellow circles and the black curve represent the experimental and theoretical results, respectively. Note that the theoretical results are multiplied by 10^6. In all panels, the experimental results are the same as those shown in Fig. 3(b) in Ref. [7].

resistance shown in Fig. 2(a) of Ref. [7]. The parameters are determined as $M_s = 0.93$ MA/m, $\mu_0 H_k = 1.0$ mT, $\mu_0 H_p = 2.15$ mT, $R_0 = 10.7$ Ω, $\bar{R} = 10.3$ Ω, and $P^2 = 0.74$. Figure 3(a) shows the bias field, $\mu_0 H_b$, dependence of the sensitivity defined as

$$\text{sensitivity} = \frac{1}{R_{\max}} \frac{dR}{d(\mu_0 H_b)}, \tag{46}$$

where $R_{\max}$ is the maximum value of the resistance. The experimental results indicated by the yellow curves are well reproduced by the theoretical results represented by the black curves.

Figure 3(b) shows the bias field dependence of the Hooge parameter, α_H. The experimental results are indicated by the yellow circles. The black solid curve represents the theoretical results multiplied by 10^6. For calculation of the Hooge parameter, the following parameters are assumed: $\alpha = 0.05$, $d = 2$ nm, $\tau_{c,\max} = 1$ s, and $T = 300$ K. The field dependences of the Hooge parameter and the sensitivity look very similar because the Hooge parameter is proportional to the square of the sensitivity along the y' axis, as indicated by Eqs. (6), (42), and (46).

The results show that the Hooge parameter of a tiny TMR sensor is much smaller than that of the conventional TMR sensor with the same sensitivity by a factor of 10^{-6}. If a number of tiny MTJs are connected in parallel to reproduce the same resistance as a conventional TMR sensor, the power spectrum of the magnetic $1/f$ noise can be reduced by a factor of 10^{-6} without reducing sensitivity.

IV. SUMMARY

In summary, we propose a theoretical model for magnetic $1/f$ noise of a tiny TMR sensor originating from a distribution of bath correlation times. Starting from the generalized Langevin equation, we derive an analytical expression for the low-frequency power spectrum of voltage. Assuming a wide distribution of the bath correlation times, the derived voltage power spectrum is inversely proportional to the frequency. We also show that the Hooge parameter of a tiny TMR sensor is much smaller than that of a conventional TMR sensor with large junction area. The power spectrum of the $1/f$ noise can be reduced substantially without reducing sensitivity by connecting tiny TMR sensors in parallel. The result provides a new perspective on magnetic $1/f$ noise and will be useful for reduction of $1/f$ noise of TMR sensors. The presented theoretical framework is applicable not only to the magnetic $1/f$ noise of a tiny TMR sensor, but also to the low-frequency fluctuation of any tiny magnetic devices where the macrospin model is appropriate.

ACKNOWLEDGMENTS

The authors thank T. Nakatani for providing experimental data and for valuable discussions. This work was partly supported by JSPS KAKENHI Grant No. JP23K04575.

Appendix: Derivation of Eqs. (22) and (23)

In this section, we provide the details of the derivation of Eqs. (22) and (23). Following Ref. [32], different approaches are used depending on the value of τ_c: in the short-τ_c regime and in the long-τ_c regime. Introducing $\xi_0 = \tau_c \omega_0$ and $\xi_1 = \tau_c \omega_1$, the short-τ_c regime is defined as $\xi_0 \xi_1 < 1$, and the long-τ_c regime is defined as $\xi_0 \xi_1 > 1$. For both τ_c regimes, we can derive the same equations of motion as Eqs. (22) and (23).

1. Short-τ_c regime: $\xi_0 \xi_1 < 1$

We approximate the non-Markovian damping term in Eq. (17) up to the first order of α. On successive application of integration by parts using $\nu(t-t') = \tau_c[d\nu(t-t')/dt']$, the integral part of the non-Markovian damping term in Eq. (17) is expressed as

$$\int_{-\infty}^{t} \nu(t-t')\dot{m}_{y'}(t')\,dt' = \sum_{n=1}^{\infty} (-\tau_c)^{n-1} \frac{d^n}{dt^n} m_{y'}(t). \tag{A1}$$

Since the integral part of the non-Markovian damping is multiplied by α, we approximate the time derivative of $m_{y'}(t)$ in the zeroth order of α as

$$\frac{d^{2n}}{dt^{2n}} m_{y'}(t) = (-1)^n \omega_0^n \omega_1^n m_{y'}(t) \tag{A2}$$

and

$$\frac{d^{2n+1}}{dt^{2n+1}} m_{y'}(t) = (-1)^n \omega_0^n \omega_1^{n+1} m_x(t). \tag{A3}$$

Substituting Eqs. (A2) and (A3) into Eq. (A1), the integral part of the non-Markovian damping term in Eq. (17) is expressed as

$$\begin{aligned}\int_{-\infty}^{t} \nu(t-t')\dot{m}_{y'}(t')\,dt' \\ = [\xi_1\omega_0 m_{y'}(t) + \omega_1 m_x(t)] \sum_{n=1}^{\infty} (-\xi_0\xi_1)^{n-1}.\end{aligned} \tag{A4}$$

The summation in Eq. (A4) converges under the condition $\xi_0\xi_1 < 1$ as

$$\sum_{n=1}^{\infty} (-\xi_0\xi_1)^{n-1} = \frac{1}{1+\xi_0\xi_1}. \tag{A5}$$

Then Eq. (A4) becomes

$$\int_{-\infty}^{t} \nu(t-t')\dot{m}_{y'}(t')\,dt' = \frac{\xi_1\omega_0 m_{y'}(t) + \omega_1 m_x(t)}{1+\xi_0\xi_1}. \tag{A6}$$

Substituting Eq. (A6) into Eq. (17) and performing some algebra, we obtain the following linearized equation of motion for $m_x(t)$ up to the first order of α:

$$\begin{aligned}\dot{m}_x(t) = &-\left(1 + \frac{\alpha\xi_1}{1+\xi_0\xi_1}\right)\omega_0 m_{y'}(t) \\ &+ \gamma r_{y'}(t) - \frac{\alpha}{1+\xi_0\xi_1}\omega_1 m_x(t).\end{aligned} \tag{A7}$$

Similarly, the following linearized equation of motion for $m_{y'}(t)$ up to the first order of α is obtained as

$$\begin{aligned}\dot{m}_{y'}(t) = &\left(1 + \frac{\alpha\xi_0}{1+\xi_0\xi_1}\right)\omega_1 m_x(t) \\ &- \gamma r_x(t) - \frac{\alpha}{1+\xi_0\xi_1}\omega_0 m_{y'}(t).\end{aligned} \tag{A8}$$

Using the symbols defined by Eqs. (24), (25), and (26), one can easily confirm that Eqs. (A7) and (A8) are the same as Eqs. (22) and (23), respectively.

2. Long-τ_c regime: $\xi_0\xi_1 > 1$

In the long-bath-τ_c regime satisfying $\xi_0\xi_1 > 1$, we expand Eq. (17) in power series of $1/(\xi_0\xi_1)$. Using integration by parts with $d\nu(t-t')/dt' = \nu(t-t')/\tau_c$, the integral part of the non-Markovian damping in Eq. (17) can be written as

$$\begin{aligned}&\int_{-\infty}^{t} \nu(t-t')\dot{m}_{y'}(t')\,dt' \\ &= \frac{1}{\tau_c}\int_{-\infty}^{t} \dot{m}_{y'}(t')\,dt' \\ &\quad - \frac{1}{\tau_c}\int_{-\infty}^{t} \nu(t-t')\left[\int_{-\infty}^{t'} \dot{m}_{y'}(t'')\,dt''\right] dt'.\end{aligned} \tag{A9}$$

Successive application of integration by parts gives

$$\int_{-\infty}^{t} \nu(t-t')\dot{m}_{y'}(t')\,dt' = -\sum_{n=1}^{\infty}\left(-\frac{1}{\tau_c}\right)^n J_n, \tag{A10}$$

where J_n is the nth-order multiple integral defined as

$$J_n = \int_{-\infty}^{t}\int_{-\infty}^{t_1}\cdots\int_{-\infty}^{t_{n-1}} \dot{m}_{y'}(t_n)\,dt_n \cdots dt_2\,dt_1. \tag{A11}$$

From Eq. (A2), on the other hand, $\dot{m}_{y'}(t)$ is expressed as

$$\dot{m}_{y'}(t) = \frac{1}{(-1)^n\omega_0^n\omega_1^n}\left(\frac{d^{2n+1}}{dt^{2n+1}} m_{y'}(t)\right). \tag{A12}$$

Substituting Eq. (A12) into Eq. (A11), the multiple integrals are calculated as

$$J_{2n} = \frac{1}{(-1)^n\omega_0^n\omega_1^n}\dot{m}_{y'}(t) \tag{A13}$$

and

$$J_{2n-1} = \frac{1}{(-1)^n\omega_0^n\omega_1^n}\ddot{m}_{y'}(t). \tag{A14}$$

Substituting the time derivative of $m_{y'}(t)$ in the zeroth order of α into Eqs. (A13) and (A14), we obtain

$$J_{2n} = \frac{\omega_1 m_x(t)}{(-1)^n\omega_0^n\omega_1^n} \tag{A15}$$

and

$$J_{2n-1} = \frac{m_{y'}(t)}{(-1)^{n-1}\omega_0^{n-1}\omega_1^{n-1}}. \tag{A16}$$

Substituting Eqs. (A15) and (A16) into Eq. (A10) and performing some algebra, the integral part of the non-Markovian damping in Eq. (17) can be expressed as

$$\begin{aligned}
&\int_{-\infty}^{t} \nu(t-t')\dot{m}_{y'}(t')\,dt' \\
&= -\sum_{n=1}^{\infty}\left[\left(-\frac{1}{\tau_c}\right)^{2n-1} J_{2n-1} + \left(-\frac{1}{\tau_c}\right)^{2n} J_{2n}\right] \\
&= -\left[\sum_{n=1}^{\infty}\left(-\frac{1}{\xi_0\xi_1}\right)^{n}\right][\xi_1\omega_0 m_{y'}(t) + \omega_1 m_x(t)] \\
&= \frac{1}{1+\xi_0\xi_1}[\xi_1\omega_0 m_{y'}(t) + \omega_1 m_x(t)]. \qquad \text{(A17)}
\end{aligned}$$

In the last equality, we use the following relation:

$$\sum_{n=1}^{\infty}\left(-\frac{1}{\xi_0\xi_1}\right)^{n} = -\frac{1}{1+\xi_0\xi_1}, \qquad \text{(A18)}$$

which holds under the condition that $\xi_0\xi_1 > 1$. Equation (A17) is the same as Eq. (A6). Substituting Eq. (A17) into Eq. (17) and performing some algebra, we obtain the same linearized equation of motion of $m_x(t)$ as Eq. (22). Equation (23) can also be obtained by similar calculations.

[1] P. P. Freitas, R. Ferreira, S. Cardoso, and F. Cardoso, Magnetoresistive sensors, J. Phys.: Condens. Matter **19**, 165221 (2007).

[2] W. Egelhoff, P. Pong, J. Unguris, R. McMichael, E. Nowak, A. Edelstein, J. Burnette, and G. Fischer, Critical challenges for picotesla magnetic-tunnel-junction sensors, Sens. Actuators, A **155**, 217 (2009).

[3] Z. Q. Lei, G. J. Li, W. F. Egelhoff, P. T. Lai, and P. W. T. Pong, Review of noise sources in magnetic tunnel junction sensors, IEEE Trans. Magn. **47**, 602 (2011).

[4] K. Fujiwara, M. Oogane, A. Kanno, M. Imada, J. Jono, T. Terauchi, T. Okuno, Y. Aritomi, M. Morikawa, M. Tsuchida, N. Nakasato, and Y. Ando, Magnetocardiography and magnetoencephalography measurements at room temperature using tunnel magneto-resistance sensors, Appl. Phys. Express **11**, 023001 (2018).

[5] M. Wang, Y. Wang, L. Peng, and C. Ye, Measurement of triaxial magnetocardiography using high sensitivity tunnel magnetoresistance sensor, IEEE Sens. J. **19**, 9610 (2019).

[6] M. Oogane, K. Fujiwara, A. Kanno, T. Nakano, H. Wagatsuma, T. Arimoto, S. Mizukami, S. Kumagai, H. Matsuzaki, N. Nakasato, and Y. Ando, Sub-pT magnetic field detection by tunnel magneto-resistive sensors, Appl. Phys. Express **14**, 123002 (2021).

[7] T. Nakatani, H. Suto, P. D. Kulkarni, H. Iwasaki, and Y. Sakuraba, Tunnel magnetoresistance sensors with symmetric resistance-field response and noise properties under AC magnetic field modulation, Appl. Phys. Lett. **121**, 192406 (2022).

[8] M. Julliere, Tunneling between ferromagnetic films, Phys. Lett. A **54**, 225 (1975).

[9] S. Maekawa and U. Gafvert, Electron tunneling between ferromagnetic films, IEEE Trans. Magn. **18**, 707 (1982).

[10] T. Miyazaki and N. Tezuka, Giant magnetic tunneling effect in $Fe/Al_2O_3/Fe$ junction, J. Magn. Magn. Mater. **139**, L231 (1995).

[11] S. S. P. Parkin, C. Kaiser, A. Panchula, P. M. Rice, B. Hughes, M. Samant, and S.-H. Yang, Giant tunnelling magnetoresistance at room temperature with MgO (100) tunnel barriers, Nat. Mater. **3**, 862 (2004).

[12] S. Yuasa, T. Nagahama, A. Fukushima, Y. Suzuki, and K. Ando, Giant room-temperature magnetoresistance in single-crystal Fe/MgO/Fe magnetic tunnel junctions, Nat. Mater. **3**, 868 (2004).

[13] M. Pannetier, C. Fermon, G. L. Goff, J. Simola, E. Kerr, and J. Coey, Noise in small magnetic systems – Applications to very sensitive magnetoresistive sensors, J. Magn. Magn. Mater. **290–291**, 1158 (2005).

[14] A. L. McWhorter, *1/f Noise and Germanium Surface Properties* (University of Pennsylvania Press, Philadelphia, 1957), p. 207.

[15] F. N. Hooge, T. G. M. Kleinpenning, and L. K. J. Vandamme, Experimental studies on $1/f$ noise, Rep. Prog. Phys. **44**, 479 (1981).

[16] P. Dutta and P. M. Horn, Low-frequency fluctuations in solids: $1/f$ noise, Rev. Mod. Phys. **53**, 497 (1981).

[17] M. B. Weissman, $1/f$ noise and other slow, non exponential kinetics in condensed matter, Rev. Mod. Phys. **60**, 537 (1988).

[18] J. Bernamont, Fluctuations in the resistance of thin films, Proc. Phys. Soc. **49**, 138 (1937).

[19] F. K. Du Pré, A suggestion regarding the spectral density of flicker noise, Phys. Rev. **78**, 615 (1950).

[20] A. Van Der Ziel, On the noise spectra of semi-conductor noise and of flicker effect, Physica **16**, 359 (1950).

[21] S. Ingvarsson, G. Xiao, S. S. P. Parkin, W. J. Gallagher, G. Grinstein, and R. H. Koch, Low-Frequency Magnetic Noise in Micron-Scale Magnetic Tunnel Junctions, Phys. Rev. Lett. **85**, 3289 (2000).

[22] C. Ren, X. Liu, B. D. Schrag, and G. Xiao, Low-frequency magnetic noise in magnetic tunnel junctions, Phys. Rev. B **69**, 104405 (2004).

[23] L. Jiang, E. R. Nowak, P. E. Scott, J. Johnson, J. M. Slaughter, J. J. Sun, and R. W. Dave, Low-frequency magnetic and resistance noise in magnetic tunnel junctions, Phys. Rev. B **69**, 054407 (2004).

[24] A. Gokce, E. R. Nowak, S. H. Yang, and S. S. P. Parkin, $1/f$ noise in magnetic tunnel junctions with MgO tunnel barriers, J. Appl. Phys. **99**, 08A906 (2006).

[25] J. M. Almeida, R. Ferreira, P. P. Freitas, J. Langer, B. Ocker, and W. Maass, $1/f$ noise in linearized low resistance MgO magnetic tunnel junctions, J. Appl. Phys. **99**, 08B314 (2006).

[26] Ana V. Silva, Diana C. Leitao, João Valadeiro, José Amaral, Paulo P. Freitas, and Susana Cardoso, Linearization strategies for high sensitivity magnetoresistive sensors, Eur. Phys. J. Appl. Phys. **72**, 10601 (2015).

[27] M. J. Garcia, J. Moulin, S. Wittrock, S. Tsunegi, K. Yakushiji, A. Fukushima, H. Kubota, S. Yuasa, U. Ebels, M. Pannetier-Lecoeur, C. Fermon, R. Lebrun, P. Bortolotti, A. Solignac, and V. Cros, Spin-torque dynamics for noise reduction in vortex-based sensors, Appl. Phys. Lett. **118**, 122401 (2021).

[28] F. Matos, R. Macedo, P. P. Freitas, and S. Cardoso, CoFeBX layers for MgO-based magnetic tunnel junction sensors with improved magnetoresistance and noise performance, AIP Adv. **13**, 025108 (2023).

[29] J. Inoue and S. Maekawa, Theory of tunneling magnetoresistance in granular magnetic films, Phys. Rev. B **53**, R11927 (1996).

[30] A. Kawabata, Brownian motion of a classical spin, Prog. Theor. Phys. **48**, 2237 (1972).

[31] K. Miyazaki and K. Seki, Brownian motion of spins revisited, J. Chem. Phys. **108**, 7052 (1998).

[32] H. Imamura, H. Arai, R. Matsumoto, T. Yamaji, and H. Tsukahara, Precession dynamics of a small magnet with non-Markovian damping: Theoretical proposal for an experiment to determine the correlation time, J. Magn. Magn. Mater. **553**, 169209 (2022).

[33] W. F. Brown, Thermal fluctuations of a single-domain particle, Phys. Rev. **130**, 1677 (1963).

[34] R. Kubo, The fluctuation-dissipation theorem, Rep. Prog. Phys. **29**, 306 (1966).

[35] H. T. Hardner, M. B. Weissman, M. B. Salamon, and S. S. P. Parkin, Fluctuation-dissipation relation for giant magnetoresistive $1/f$ noise, Phys. Rev. B **48**, 16156 (1993).

[36] N. Smith, Modeling of thermal magnetization fluctuations in thin-film magnetic devices, J. Appl. Phys. **90**, 5768 (2001).

[37] V. L. Safonov and H. N. Bertram, Nonuniform thermal magnetization noise in thin films: Application to GMR heads, J. Appl. Phys. **91**, 7279 (2002).

[38] A. Ozbay, A. Gokce, T. Flanagan, R. A. Stearrett, E. R. Nowak, and C. Nordman, Low frequency magnetoresistive noise in spin-valve structures, Appl. Phys. Lett. **94**, 202506 (2009).